Electrochemical Properties of Iron Oxide Nanoparticles as an Anode for Li-ion Batteries

Mohammad Golmohammad[a,b,*] , Farhad Golestanifard[a], Alireza Mirhabibi[a,c]

[a] *School of Metallurgy and Materials Engineering, Iran University of Science and Technology (IUST), Tehran, Iran*
[b] *Faculty of Applied Sciences, Delft University of Technology, Delft, Netherlands*
[c] *Institute for Materials Research (IMR), University of Leeds, Leeds, United Kingdom*

ARTICLE INFO

ABSTRACT

The synthesis of iron oxide nano-particles by direct thermal decomposition was studied. Simultaneous thermal analysis and Fourier transform infrared spectroscopy results confirmed the formation of iron-urea complex and disclosed iron oxide formation mechanism. Calcination of the iron-urea complex at 200°C and 250°C for 2 h resulted in the formation of maghemite along with hematite as a second phase. X-ray diffraction (XRD) results revealed that increment of iron-urea complex calcination temperature led to the augmentation of hematite to maghemite ratio. Field emission scanning electron microscopy (FE-SEM) and transmission electron microscopy (TEM) results showed that the average particle size was around 38nm for the sample calcined at 250°C for 2 hrs. The anode body was doctor bladed using primary powder with polyvinylidene difluoride and graphite. Galvanostatic charge–discharge cycling showed a reversible capacity of 483 mAh g^{-1} at 100 mA g^{-1} current density. The reason for this competent performance was thought to be dependent upon the particle sizes.

1. Introduction

In recent years, iron oxide nano-particles have found different applications such as drug delivery [1, 2], catalysis [3, 4], ferrofluids [5, 6], and Li-ion batteries [7-15]. There are different methods to synthesize iron oxides nano-particles, including hydrothermal[16, 17], microemultion [18], co-precipitation [5, 14, 19, and 20], thermal decomposition [21-24], and microwave synthesis [25]. In the past decade, thermal decomposition showed promising ability to synthesize crystalline nano iron oxides. Heyon et al. have synthesized nano maghemite using pentacarbonyl iron $(Fe(CO)_5)$ and actyl ether [23]. Sun and Zeng have synthesized nano maghemite using high temperature reaction of acytelene acetone Iron [21]. However, both of these methods utilize toxic raw material and additionally they are not single step methods. In the present study, we have used a single step thermal decomposition method to synthesize iron oxide nano-particles.

As mentioned earlier, recently iron oxides are considered as electrodes for Li-ion battery because of their high capacity as well as their low cost, non-toxicity and availability. The high capacity of iron oxides results from the reversible conversion reaction between lithium ions (Li^+) and iron oxides (Fe_xO_y), as shown by Eq. (1).

$$Fe_xO_y + 2yLi^+ + 2ye^- \leftrightarrow xFe + yLi_2O \qquad (1)$$
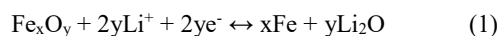
The different types of iron oxides such as hematite $(\alpha\text{-}Fe_2O_3)$ [9-11], maghemite $(\gamma\text{-}Fe_2O_3)$ [7,8, and 14], and magnetite (Fe_3O_4) [12,13, and 15] have been studied as an electrode. The main impasses are capacity

* Corresponding Author:
  E-mail Address: m_golmohammad@iust.ac.ir

fading during the charge-discharge and low initial coulombic efficiency, which are caused by low electrical conductivity and a drastic volume change during the charge-discharge process. One of the main solutions to these drawbacks is using nano-particles which can improve the performance of iron oxide as an electrode. Different nanostructures of hematite, magnetite and maghemite have been synthesized to improve their electrochemical properties. However, most of them use multi-step and complicated methods to synthesize iron oxide.

In this work, iron oxide was synthesized by single-step thermal decomposition method and the electrochemical properties of nano-sized iron oxide as a Li-ion battery electrode were investigated.

2. Experimental Procedure
2.1. Materials
Iron (III) nitrate nonahydrate ($Fe(NO_3)_3.9H_2O$), urea and ethanol were all chemical grades and obtained from Sigma-Aldrich. All the chemicals were used "as received" without any further purification.

2.2. Synthesis of iron oxide
A solution of $Fe(NO_3)_3.9H_2O$ and urea were mixed at the molar ratio of 1:6.2 in ethanol at room temperature and stirred for 30min until a green powder were obtained. This green precipitate was separated by filtering and rinsed with ethanol several times. The obtained powders were dried at 60°C and heated at 200°C and 250°C to synthesize iron oxide.

2.3. Characterization
X-ray diffraction (XRD) measurements were carried out with a Bruker (AXS D8 Advance) using Co-K_α radiation. The microstructure and morphology of the samples were recorded using a transmission electron microscope (TEM, Philips EM201C) and field emission scanning electron microscopy (FE-SEM, TESCAN). Simultaneous thermal analysis (STA) was conducted with an STA Instrument 2960. Fourier transform infrared spectroscopy (FTIR) was carried out using Perking-Elmer Spectrum 100.

2.4. Electrochemical Evaluation

For preparation of the electrode, optimized powder was milled and mixed with graphite and polyvinylidene difluoride powder (PVdF - Solef) in a weight ratio of 15:3:2 using N-methyl pyrrolidone (NMP - Merk-Schuchardt) as the dissolving solvent. The mixture was mixed for 1h to form a homogeneous slurry, and then was doctor bladed on an etched copper foil as current collector up to a thickness of 100μm. The copper foil was then dried at 110°C and circular disks (14mm in diameter) were punched out which then served as the test electrodes. Metallic lithium disks were used as reference and counter electrode and 1M $LiPF_6$ dissolved in ethylene carbonate (EC) and dimethyl carbonate (DMC) (2:1 by wt. – Mitsubishi Chemicals) as the electrolyte. These electrodes were stacked together in a CR2320 coin cell (Hohsen) assembled in an Ar-filled glove-box (MBraun). Galvanostatic tests were performed with a Maccor cycler (S-4000) and the cycling performance and capacity was monitored. Before the electrochemical measurements, the cells were aged for 12 hrs. The voltage limits were set to 0.01 and 3 V vs Li/Li^+.

3. Result and discussion
The STA pattern of the synthesized powder is presented in Fig. 1. The thermogravimetric result curve shows two distinct transitions between room temperature and 600°C with a total weight loss of roughly 90%. The first endothermic peak at 182°C is due to the melting of iron-urea complex. The first weight loss was 72% between 198-203°C in accordance with a sharp exothermic peak in the differential thermal analysis curve at 200°C. This exothermic peak is because of iron-urea complex decomposition and iron oxide formation. The second weight loss is 18% between 240°C and 265°C in accordance with an exothermic peak at 255°C which is due to the burning of residual components.
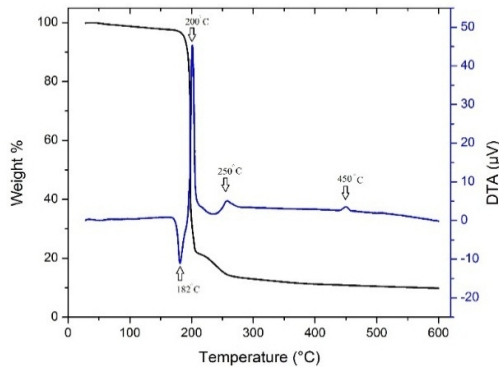
Fi. 1. STA result of the as-synthesized powder.

Another exothermic peak at 450°C is attributed to the transformation of residual maghemite to hematite. For better understanding of this phenomenon, the as-synthesized powder was heated at 200°C

(T200) and 250°C (T250) for 2 h and FTIR tests were carried out. In the infrared spectra of urea and as-synthesized powder, the following three large changes were clearly observed: (1) the absorption band at 1676 cm^{-1}, which was attributable to CO stretching vibration, shifted to 1624 cm^{-1}, (2) the band at 1462 cm^{-1}, which was attributable to C–N stretching vibration, shifted to 1496 cm^{-1}, (3) a new strong band was observed at 1385 cm^{-1}, which was a characteristic absorption band of NO3$^-$. Decrease of the CO stretching frequency and an increase in the CN stretching one indicate that the metal ion is coordinated to urea through oxygen atoms [24].
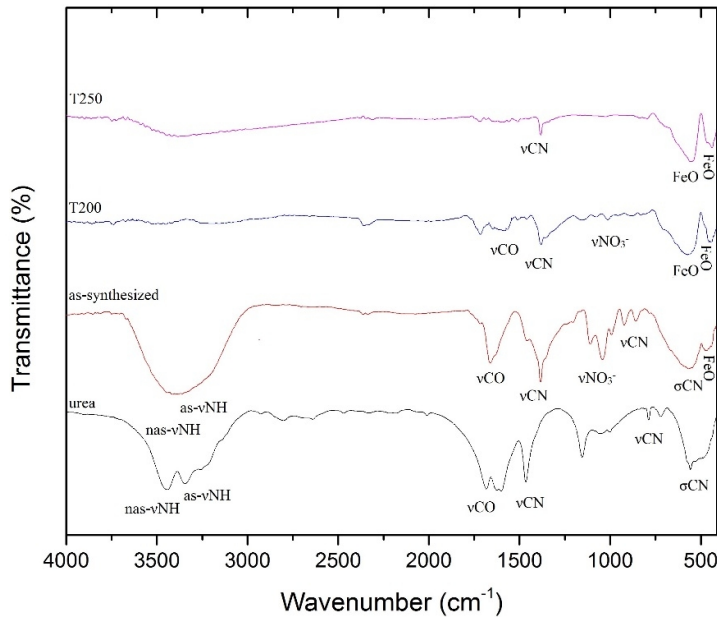
Fig 2. The FTIR result of urea, as-synthesized, T200 and T250 powders.

For sample T200, there are bands at 446, 695cm^{-1} which are attributable to maghemite and a broad band at 566cm^{-1} attributed to hematite [14]. Increment of heating temperature led to the elimination of the band at 695cm^{-1} and appearing of a new band at 480 cm^{-1} (attributed to hematite) which proposed increasing in hematite ratio. Also for sample T200, there is a weak peak of NO3$^-$, while with heating the sample at 250°C, there is no sign of that band anymore.

Regarding the results of STA and FTIR, the following reactions can be concluded:

$$F^{3+} + 6C\ N_2H_4 + 3NO_3^- \leftrightarrow$$
$$[F\ (C\ N_2H_4)_6](NO_3)_3 \quad (2)$$
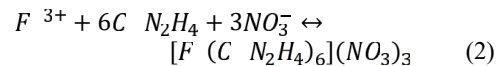
As can be seen, with increasing heating temperature to 200°C, there is still the band of NO3$^-$ but it is weaker. This result confirms the mechanism suggested by Carp et al. [24]. According to them, at the first stage after melting of iron-urea complex, a

simultaneously release of nitrate urea and NO_2 take place:

$$[F\ (C\ N_2H_4)_6](NO_3)_3 \rightarrow$$
$$[F\ (C\ N_2H_4)_6](NO_3)_{3-x} \qquad (3)$$

$$[F\ (C\ N_2H_4)_6](NO_3)_{3-x} \rightarrow$$
$$F\ ^{3+}+(NO_3^{-})_{3-x}+6C\ N_2H_4 (4)$$

$$2F\ ^{3+}+2x\ H^- \rightarrow 2F\ (O\ )_x + O_2 \rightarrow$$
$$F\ _2O_3(\alpha,\gamma)+xH_2O \qquad (5)$$
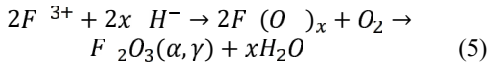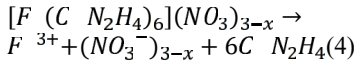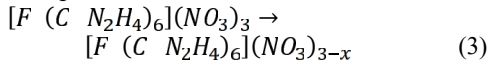
On the other hand, the thermal decomposition product medium partially reduces the iron ions, which leads to the formation of iron hydroxides and oxyhydroxides. In the next stage, iron hydroxide would be transformed to maghemite as well as hematite.

Figure 3 shows the diffraction pattern of T200 and T250 samples which agrees well with the JCPDS - International Centre for Diffraction Data® file (No. 39-1346) of γ-Fe_2O_3 as the main phase and hematite (α-Fe_2O_3, JCPDS No. 33-0664) as the second phase. These results are in good agreement with FTIR results and confirm the suggested mechanism. It can be seen that with increasing the heating temperature, the hematite phase increases which was predictable. The crystallite size calculated by the Debye-Scherrer equation revealed 15±0.2 nm for T200 and 17±0.3 nm for T250.
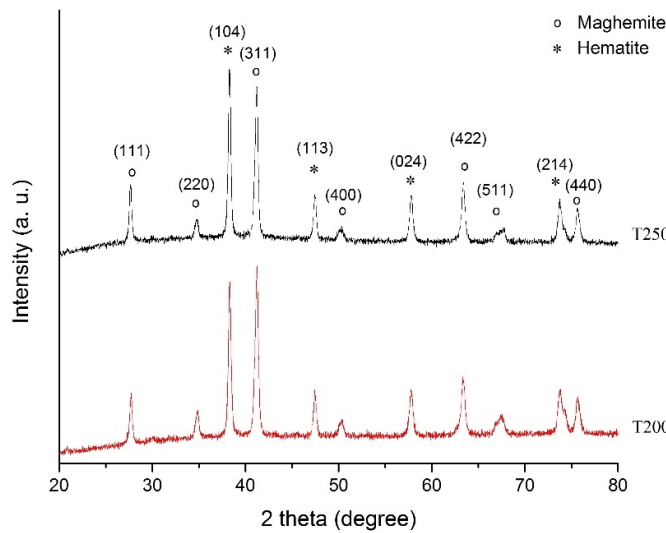
Fig 3. XRD pattern of the T200 and T250 samples.

These results are in good agreement with the result of carp et al. [24] and contrary to the results of Asuha et al.[22] . Asuha et al. claimed that they had synthesized maghemite as a single phase with the same method which is in contrast with our work. Regarding the fact that thermal decomposition reactions occur in unstable condition at air, it seems not likely to have maghemite as a single phase.

Figure 4 shows FESEM and TEM images of the T250 sample. The particles were agglomerated due to heating and combustion of iron urea complex. The average particle size is around 38nm for nanoparticles synthesized by thermal decomposition method. TEM of this powder demonstrates that the particles do not have a defined shape and shows particles with different sizes.
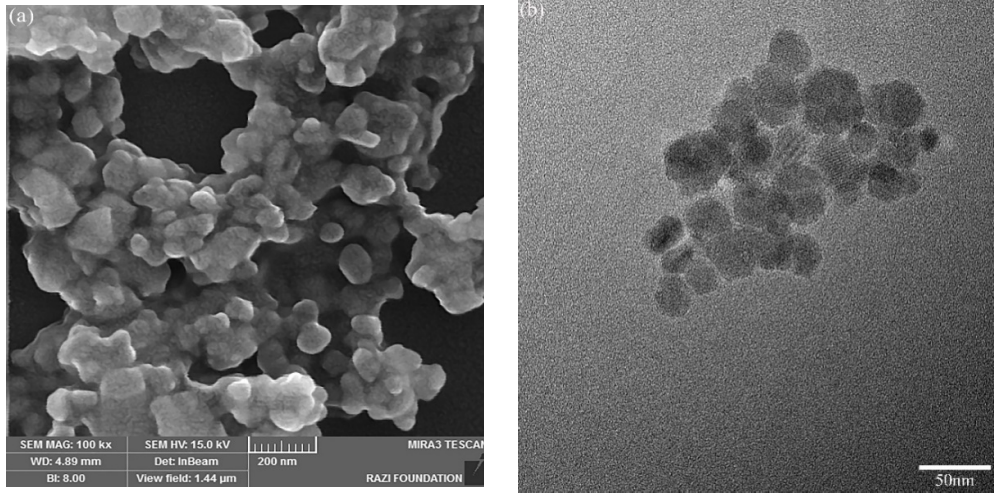
Fig 4. Morphology of the T250 sample (a) FESEM (b) TEM.

The insertion–extraction cycles were carried out at $100 mAg^{-1}$ current density to investigate the electrochemical behavior of the anode, which has been shown in Fig. 5. The voltage profile for the first insertion cycle had three distinct features (Fig. 5 (a)). The step voltage dropped to 1.6 V or so with a small plateau refers to the intercalation of Li ions with iron oxide structure which leads to the formation of an Li–Fe–O complex according to Eq. (6). There is another voltage plateau at about 0.8 V which refers to the conversion reaction of the Li–Fe–O complex to Li_2O and Fe (Eq. (7)). The gradual voltage decay from 0.7 V to 0.01 V is related to the formation of a gel like anode electrolyte interface called solid electrolyte interphase (SEI) [10].

$$Fe_2O_3 + xLi = Li_xFe_2O_3 \qquad (6)$$

$$Li_xFe_2O_3 + (6 - x)Li = 2Fe + 3Li_2O \qquad (7)$$
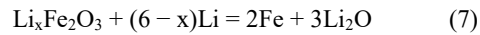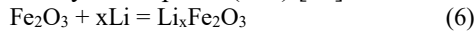
Total capacity of 1380 mAh g^{-1} was delivered for the T250 sample at the first cycle during the insertion, and the reversible capacity was 483 mAh g^{-1} after 50 cycles. The theoretical capacity of Fe_2O_3 is 1006 mAh g^{-1} and the extra capacity in the first cycle is due to the SEI formation which has been observed by other researchers as well [9, 10]. For the fiftieth cycle, the two first steps still exist while the capacity decreased; however, the third part from 0.7 V to 0.01 V faded because the SEI is a passive layer and, as a consequence, its formation would stop after the first cycle.
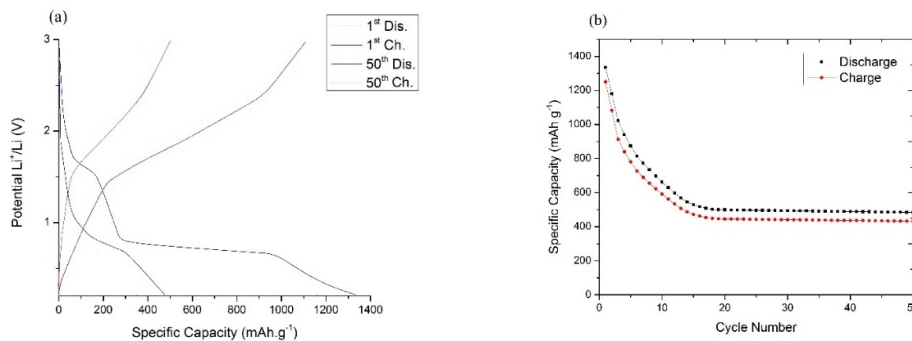
Fig 5. Electrochemical properties of T250 sample (a) Potential Li+/Li vs. Specific capacity (b) Specific capacity Vs. Cycle number.

Figure 5 (b) shows the discharge-charge capacities of the cycle numbers for the T250 sample at a current density of 100 mA g^{-1}. The T250 sample showed a good electrochemical

performance as high reversible capacity and cyclability compared to the results of previous researches, which benefited from smaller particle size [8], [10]. Normally, the pulverization process takes place because of the large volume swing generated during the Li ions insertion and extraction process that leads to the disintegration of electrodes and hence a loss of electrical contacts[10]; this electrical contact loss is the main reason for the capacity loss in the first cycles. It can be seen that after 15 cycles or so, the total capacity remained unchanged.

The current work showed good cycling performance amongst similar cells made from iron oxide nanoparticles, carbon black and binders [7, 8, 26, and 27]. These counterparts showed reversible capacity of 400 mAh g^{-1}, 450 mAh g^{-1}[8], 200 mAh g^{-1} [26], and 190 mAh g^{-1} [27] at current density of 50, 100, 200, and 500 mA g^{-1}, respectively.

This result is as good as anode made of iron oxide and graphene [15]. However, graphene acts as conducting agents and structural buffers in the anode structure thereby imparting high rate capability and structural stability. But the current results, based on a conventional anode configuration, indicate that control of nanoparticle size can improve the cell performance.

4. Conclusion

The iron oxide nano-particles were synthesized via thermal decomposition of iron-urea complex. STA and FTIR results revealed that thermal decomposition of iron-urea complex led to the removal of urea and NO_2 gaseous and formation of iron hydroxide at roughly 200°C. In the next stage, iron hydroxide transformed to maghemite and hematite. XRD result showed that crystalline iron oxides can be formed with heating iron-urea complex in air at 200°C. The crystalline iron oxide is a mixture of maghemite and hematite, and the ratio of hematite will be increased with augmentation of heating temperature. The XRD, FESEM and TEM results related to the iron-urea complex heated at 250°C showed the average crystallite and particle size of 17 and 38 nm, respectively. Electrochemical characterization of the nanopowders for the Li-ion battery anodes showed the first discharge

capacity of ~1380 mAh g^{-1} and the reversible discharge capacity of ~483 mAh g^{-1} at a current density of 100 mA g^{-1}. The good cyclability, capacity retention and rate capability of the anode is attributed to the nanometric size of the iron oxide particles.

References

[1] P. Guardia, N. Pérez, A. Labarta, and X. Batlle, "Controlled synthesis of iron oxide nanoparticles over a wide size range", Langmuir, vol. 26, 2010, pp. 5843–5847.

[2] M. Mahdavi, M. Bin Ahmad, M. J. Haron, F. Namvar, B. Nadi, M. Z. A. Rahman, and J. Amin, "Synthesis, surface modification and characterisation of biocompatible magnetic iron oxide nanoparticles for biomedical applications", Molecules, vol. 18, 2013, pp. 7533–7548.

[3] R. Bonelli, S. Albonetti, V. Morandi, L. Ortolani, P. M. Riccobene, S. Scirè, and S. Zacchini, "Design of nano-sized FeOx and Au/FeOx catalysts supported on CeO2 for total oxidation of VOC," Appl. Catal. A Gen., vol. 395, 2011, pp. 10–18.

[4] F. Mou, J. Guan, W. Shi, Z. Sun, and S. Wang, "Oriented contraction: a facile nonequilibrium heat-treatment approach for fabrication of maghemite fiber-in-tube and tube-in-tube nanostructures", Langmuir, vol. 26, 2010, pp. 15580–15585.

[5] E. Ghasemi, A. Mirhabibi, and M. Edrissi, "Synthesis and rheological properties of an iron oxide ferrofluid", J. Magn. Magn. Mater., vol. 320, 2008, pp. 2635–2639.

[6] S. Charles, "The preparation of magnetic fluids", Hand book of magnetic materials, Springer-Verlag Berlin Heidelberg, 2002, pp. 3–18.

[7] Y. Wu, P. Zhu, and M. Reddy, "Maghemite Nanoparticles on Electrospun CNFs Template as Prospective Lithium-Ion Battery Anode", ACS Appl. Mater. Interfaces, vol. 6, 2014, pp. 1951–1958.

[8] O. Vargas, Á. Caballero, and J. Morales, "Enhanced Electrochemical Performance of Maghemite/Graphene Nanosheets Composite as Electrode in Half and Full Li–Ion Cells", Electrochim. Acta, vol. 130, 2014, pp. 551–558.

[9] M. Valvo, E. García-Tamayo, U. Lafont, and E. M. Kelder, "Direct synthesis and

coating of advanced nanocomposite negative electrodes for Li-ion batteries via electrospraying", J. Power Sources, vol. 196, pp. 10191–10200.

[10] D. Larcher, C. Masquelier, D. Bonnin, Y. Chabre, V. Masson, J.-B. Leriche, and J.-M. Tarascon, "Effect of Particle Size on Lithium Intercalation into α-Fe[sub 2]O[sub 3]", J. Electrochem. Soc., vol. 150, 2003, pp. A133-A139.

[11] J. Liu, W. Zhou, L. Lai, H. Yang, S. Hua Lim, Y. Zhen, T. Yu, Z. Shen, and J. Lin, "Three dimensionals α-Fe2O3/polypyrrole (Ppy) nanoarray as anode for micro lithium ion batteries", Nano Energy, vol. 2, 2013, pp. 726–732.

[12] Y. C. Dong, R. G. Ma, M. Jun Hu, H. Cheng, C. K. Tsang, Q. D. Yang, Y. Yang Li, and J. A. Zapien, "Scalable synthesis of Fe3O4 nanoparticles anchored on graphene as a high-performance anode for lithium ion batteries", J. Solid State Chem., vol. 201, 2013, pp. 330–337.

[13] L. Shi, Y. D. He, X. H. Xia, Z. M. Jian, and H. B. Liu, "High Rate Capability of Fe / FeO / Fe 3 O 4 Composite as Anode Material for Lithium-Ion Batteries", J. Iran Chem. Soc., vol. 7, 2010, pp. 721–726.

[14] M. Golmohammad, A. Mirhabibi, F. Golestanifard, E. M. Kelder, "Optimizing synthesis of maghemite nanoparticles as an anode for Li-ion batteries by exploiting design of experiment", J. Electron. Mater. Forthcoming (2015).

[15] M. Y. Li, Y. Wang, C. L. Liu, H. Gao, W.S. Dong, "Iron oxide/carbon microsphere lithium-ion battery electrode with high capacity and good cycling stability", Electrochim. Acta, vol. 67, 2012, pp. 187- 193.

[16] Y. NuLi, P. Zhang, Z. Guo, P. Munroe, and H. Liu, "Preparation of α-Fe2O3 submicro-flowers by a hydrothermal approach and their electrochemical performance in lithium-ion batteries", Electrochim. Acta, vol. 53, 2008, pp. 4213–4218.

[17] O. Horner, S. Neveu, S. Montredon, J.-M. Siaugue, and V. Cabuil, "Hydrothermal synthesis of large maghemite nanoparticles: influence of the pH on the particle size", J. Nanoparticle Res., vol. 11, 2009, pp. 1247–1250.

[18] J. Vidal-Vidal, J. Rivas, and M. a. López-Quintela, "Synthesis of monodisperse maghemite nanoparticles by the microemulsion method", Colloids Surfaces A Physicochem. Eng. Asp., vol. 288, 2006, pp. 44–51.

[19] T. Ahn, J. H. Kim, H.-M. Yang, J. W. Lee, and J.-D. Kim, "Formation Pathways of Magnetite Nanoparticles by Coprecipitation Method", J. Phys. Chem. C, vol. 116, 2012, pp. 6069–6076.

[20] S. J. Lee, J. R. Jeong, S. C. Shin, J. C. Kim, and J. D. Kim, "Synthesis and characterization of superparamagnetic maghemite nanoparticles prepared by coprecipitation technique", J. Magn. Magn. Mater., vol. 282, 2004, pp. 147–150.

[21] S. Sun, and H. Zeng, "Size-controlled synthesis of magnetite nanoparticles", J. Am. Chem. Soc., vol. 124, 2002, pp. 8204–8205.

[22] S. Asuha, S. Zhao, H. Y. Wu, L. Song, and O. Tegus, "One step synthesis of maghemite nanoparticles by direct thermal decomposition of Fe – urea complex and their properties", J. Alloys Compd., vol. 472, 2009, pp. L23–L25.

[23] T. Hyeon, S. S. Lee, J. Park, Y. Chung, and H. B. Na, "Synthesis of highly crystalline and monodisperse maghemite nanocrystallites without a size-selection process", J. Am. Chem. Soc., vol. 123, 2001, pp. 12798–801.

[24] O. Carp, L. Patron, L. Diamandescu, and A. Reller, "Thermal decomposition study of the coordination", Thermochim. Acta, vol. 390, 2002, pp. 169–177.

[25] S. Komarneni, W. Hu, Y. D. Noh, A. Van Orden, S. Feng, C. Wei, H. Pang, F. Gao, Q. Lu, and H. Katsuki, "Magnetite syntheses from room temperature to 150°C with and without microwaves", Ceram. Int., vol. 38, 2012, pp. 2563–2568.

[26] H. Morimoto, S. Tobishima, and Y. Iizuka, "Lithium intercalation into α-Fe2O3 obtained by mechanical milling of α-FeOOH", J. Power Sources, vol.146, 2005, pp. 315-318.

[27] B.T. Hang, I. Watanabe, T. Doi, S. Okada, J. I. Yamaki, "Electrochemical properties of nano-sized Fe2O3-loaded carbon as a lithium battery anode", J. Power Sources, vol. 161, 2006, pp. 1281-1287.